Available online at www.sciencedirect.com
SCIENCE DIRECT
International Journal of Heat and Mass Transfer 49 (2006) 4265–4278
International Journal of HEAT and MASS TRANSFER
www.elsevier.com/locate/ijhmt

Direct simulation of spray cooling: Effect of vapor bubble growth and liquid droplet impact on heat transfer

R. Panneer Selvam [a,*], Lancho Lin [b], Rengasamy Ponnappan [c]

[a] BELL 4190, University of Arkansas, Fayetteville, AR 72701, USA
[b] Universal Energy systems Inc., 4401 Dayton-Xenia Road, OH 45432-1894, USA
[c] Air Force Research Laboratory, Propuslion Directorate, Wright-Patterson AFB, OH 45433-7251, USA

Received 31 August 2005; received in revised form 13 May 2006
Available online 17 July 2006

Abstract

Numerical modeling of multiphase flow using level set method is discussed. The 2-D model considers the effect of surface tension between liquid and vapor, gravity, phase change and viscosity. The level set method is used to capture the movement of the free surface. The detail of incorporating the mechanism of phase change in the incompressible Navier–Stokes equations using the level set method is described. The governing equations are solved using the finite difference method. The computer model is used to study the spray cooling phenomenon in the micro environment of about 40 μm thick liquid layer with vapor bubble growing due to nucleation. The importance of studying the heat transfer mechanism in thin liquid film for spray cooling is identified. The flow and heat transfer details are presented for two cases: (1) when the vapor bubble grows due to nucleation and (2) merges with the vapor layer above the liquid layer and when a liquid droplet impacts the thin liquid layer with vapor bubble growing.

Keywords: Spray cooling; Heat transfer enhancement; Multiphase flow modeling; Level set method

1. Introduction

Spray cooling is a high flux heat removal technique considered for high power systems such as advanced lasers. The spray cooling with phase change and droplet impact can achieve heat fluxes up to 1000 W/cm^2 as reported by Yang et al. [1]. Several experiments have been conducted using spray cooling in recent years [2–4] and various designs of spray cooling devices are emerging. Theoretical understanding of the spray cooling heat acquisition phenomena is still in its infancy and a focused effort to develop a comprehensive numerical model is a prime importance to this field.

Even though spray cooling is used in the industry for several years the overall theoretical understanding is limited due to complex interaction of liquid, vapor, liquid droplet impact and phase change as sketched in Fig. 1. Only limited work is available in the related area of bubble dynamics [5,6], pool boiling [6–11], droplet impact [12,13] on a hot plate and some simplified model for spray cooling [14–16]. A detailed survey on current status of computer modeling of spray cooling and methods to solve multiphase flow is presented in Selvam and Ponnappan [17]. Recently Selvam et al. [18], and Selvam and Ponnappan [17] identified that computer modeling of nucleation boiling in thin film in the neighborhood of 70 μm including droplet impact will provide valuable information in the design of experiments for spray cooling. Preliminary computation of a growing of vapor bubble in thin film of liquid and the transient heat transfer on the wall are reported by Selvam and Ponnappan [17]. They identified that high heat transfer

* Corresponding author. Tel.: +1 479 575 5356; fax: +1 479 575 7168.
E-mail addresses: rps@engr.uark.edu, rps@uark.edu (R.P. Selvam).

0017-9310/$ - see front matter © 2006 Elsevier Ltd. All rights reserved.
doi:10.1016/j.ijheatmasstransfer.2006.05.009

Nomenclature

c_p	specific heat at constant pressure
g	gravity vector
H	step function
h	grid spacing
h_{fg}	latent heat of evaporation
Ja	Jacob number $= c_{pl}\Delta T/h_{fg}$
k	thermal conductivity
l_r	characteristic length $\sqrt{\sigma/g(\rho_l - \rho_v)}$
$\mathbf{m}$	mass flux vector
Nu	Nusselt number $ql_r/(\Delta Tkl)$
p	pressure
Pe	Peclet number $= \rho_l u_r l_r c_{pl}/k_l$
Pr	Prandtl number $= c_{pl}\mu_l/k_l$
q	heat flux
Re	Reynolds number $= \rho_l u_r l_r/\mu_l$
T	temperature
T^*	dimensionless temperature $(T - T_{sat})/(T_w - T_{sat})$
ΔT	temperature difference $T_w - T_{sat}$
t	time
t_r	characteristic time l_r/u_r
$\mathbf{u}$	velocity vector (u, v)
$\mathbf{u}_{int}$	interface velocity vector
u_r	characteristic velocity $\sqrt{gl_r}$
We	Weber number $= \rho_l u_r^2 l_r/\sigma$
α	thermal diffusivity
κ	interfacial curvature
μ	dynamic viscosity
ρ	density
σ	surface tension
φ	level set function

Subscripts

int	interface
l, v	liquid, vapor
sat, w	saturation, wall

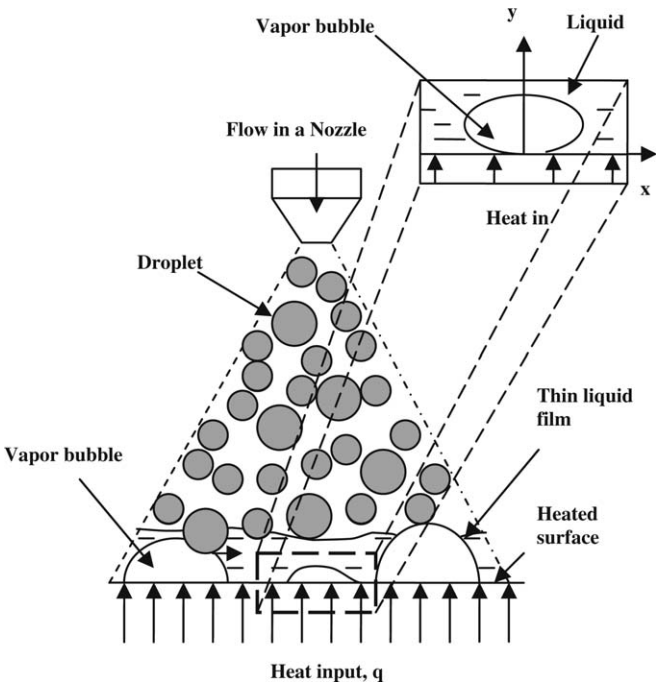

Fig. 1. Spray cooling phenomena.

takes place during the impact of liquid droplet on thin liquid film where vapor bubble is growing. The droplet impact on a growing vapor bubble in a thin film when the droplet came right over the vapor bubble is reported in Selvam et al. [18]. For this case the droplet could not collapse the vapor bubble and hence the impact on the heat transfer is minimal. Further work on computer modeling of vapor bubble merging with vapor region over the thin liquid layer due to nucleation growth and impact of liquid droplet for different positions of the droplet is reported. The heat transfer rate at different instants for each case is presented.

2. Numerical formulation for multiphase flow using level set method

For a survey on numerical techniques used to model multiphase flow and their advantages and disadvantages one can refer to the literature [6,17,18]. Here, for computer modeling of liquid and vapor during nucleate boiling, the level set method introduced by Sussman et al. [5] for bubble dynamics which was modified by Son and Dhir [7] to accommodate the effect of phase change is used. The interface separating the two phases is captured by a function φ which is defined as a positive or negative distance from the interface. Similar to Son and Dhir [7] and Son et al. [8] the negative sign is chosen for the vapor phase and the positive sign is chosen for the liquid phase. For more details on the level set method and it application one can refer to Sethian [19] and Osher and Fedikiw [20]. The extensive application of the level set method in various areas of science and engineering are illustrated with their basic development in the above two books.

2.1. Governing equations

In the present model, the fluid properties including density, viscosity and thermal conductivity are constant in each phase and the flow is assumed to be incompressible. The Navier–Stokes equations considering the effect of surface tension, gravity and phase change at the interface are as follows:

$$\rho(\partial_t \mathbf{u} + \mathbf{u}\cdot\nabla\mathbf{u}) = -\nabla p + \rho\mathbf{g} - \sigma\kappa\nabla H + \nabla\cdot\mu\nabla\mathbf{u} + \nabla\cdot\mu\nabla\mathbf{u}^{\mathrm{T}} \tag{1}$$

$$\rho c_{\mathrm{pl}}(\partial_t T + \mathbf{u}\cdot\nabla T) = \nabla\cdot k\nabla T \quad \text{for } H > 0 \text{ and } T = T_{\mathrm{sat}}(p_{\mathrm{v}}) \text{ for } H = 0 \tag{2}$$

$$\nabla\cdot\mathbf{u} = \mathbf{m}\cdot\nabla\rho/\rho^2 \tag{3}$$

where

$$\rho = \rho_{\mathrm{v}} + (\rho_{\mathrm{l}} - \rho_{\mathrm{v}})H \tag{4}$$

The value of μ and k are calculated using the similar relation in Eq. (4). Here

$$\begin{aligned} H &= 1 \quad \text{if } \varphi \geqslant 1.5h \\ &= 0 \quad \text{if } \varphi \leqslant -1.5h \\ &= 0.5 + \varphi/(3h) + \sin[2\pi\varphi/(3h)]/(2\pi) \quad \text{if } |\phi| \leqslant 1.5h \end{aligned} \tag{5}$$

where h is a grid spacing. The Eq. (5) implies that the interface separating two phases is replaced by a transition region of finite thickness. The volume source term included in the continuity equation (3) due to liquid–vapor phase change is derived from the conditions of mass continuity and energy balance at the interface:

$$m = \rho(\mathbf{u}_{\mathrm{int}} - \mathbf{u}) = k\nabla T/h_{\mathrm{fg}} \tag{6}$$

In the level set formulation, the level set function φ, is advanced and reinitialized as

$$\partial_t\varphi = -\mathbf{u}_{\mathrm{int}}\cdot\nabla\varphi \tag{7}$$

$$\partial_t\varphi = \varphi_0(1 - |\nabla\varphi|)/\sqrt{(\varphi_0^2 + h^2)} \tag{8}$$

where φ_0 is a solution of Eq. (7).

The surface tension effect is considered in the momentum equation by using a step function H ($H = 0$ in the vapor and 1 in liquid) and κ is the interfacial curvature expressed as

$$\begin{aligned} \kappa &= \nabla\cdot(\nabla\varphi/|\nabla\varphi|) \\ &= (\varphi_y^2\varphi_{xx} - 2\varphi_x\varphi_y\varphi_{xy} + \varphi_x^2\varphi_{yy})/(\varphi_x^2 + \varphi_y^2)^{3/2} \quad \text{for 2D} \end{aligned} \tag{9}$$

Here subscripts are differentiation with respect to φ. The surface tension force, $-\sigma\kappa\nabla H$ is implemented in the volume form to avoid the need for explicit description of the interface (Brackbill et al. [21]).

2.2. Nondimensional form of the governing equations

The nondimensional form of the above set of equations is derived using the characteristic length l_{r}, velocity u_{r}, time t_{r} and dimensionless temperature T^*. They are defined as follows:

$$l_{\mathrm{r}} = \sqrt{\sigma/g(\rho_{\mathrm{l}} - \rho_{\mathrm{v}})}, \quad u_{\mathrm{r}} = \sqrt{g l_{\mathrm{r}}}, \quad t_{\mathrm{r}} = l_{\mathrm{r}}/u_{\mathrm{r}} \quad \text{and} \quad T^* = (T - T_{\mathrm{sat}})/(T_{\mathrm{w}} - T_{\mathrm{sat}}) \tag{10}$$

The reference values are taken in such a way that the gravity force becomes unity that is Froude number equal to 1 and the Weber number (We) is just above 1.0 if the density ratio of the liquid to vapor is larger. In addition, considering ρ, k, μ and c_{p} of liquid as reference values, the nondimensional equations without their superscripts are expressed as follows:

$$\rho(\partial_t\mathbf{u} + \mathbf{u}\cdot\nabla\mathbf{u}) = -\nabla p + \rho g_y - \kappa\nabla H/We + (\nabla\cdot\mu\nabla\mathbf{u} + \nabla\cdot\mu\nabla\mathbf{u}^{\mathrm{T}})/Re \tag{11}$$

$$\rho c_{\mathrm{pl}}(\partial_t T + \mathbf{u}\cdot\nabla T) = (\nabla\cdot k\nabla T)/Pe \quad \text{for } H > 0 \tag{12}$$

$$\nabla\cdot\mathbf{u} = Jak\nabla T\cdot\nabla\rho/(Pe\rho^2) \tag{13}$$

$$\mathbf{u}_{\mathrm{int}} = \mathbf{u} + Jak\nabla T/(Pe\rho) \tag{14}$$

where $Re = \rho_{\mathrm{l}}u_{\mathrm{r}}l_{\mathrm{r}}/\mu_{\mathrm{l}}$, $We = \rho_{\mathrm{l}}{u_{\mathrm{r}}}^2 l_{\mathrm{r}}/\sigma$, $Ja = c_{\mathrm{pl}}\Delta T/h_{\mathrm{fg}}$, $Pr = c_{\mathrm{pl}}\mu_{\mathrm{l}}/k_{\mathrm{l}}$ and $Pe = RePr = \rho_{\mathrm{l}}u_{\mathrm{r}}l_{\mathrm{r}}c_{\mathrm{pl}}/k_{\mathrm{l}}$. Here g_y represents unit gravitational force in the y-direction. In the Eqs. (11)–(14), ρ, k, μ and c_{p} are dimensionless with respect to the reference values.

2.3. Boundary conditions

The boundary conditions for the governing equations are shown in Fig. 2 and also given below. At the wall ($y = 0$): $u = v = 0$, $T = T_{\mathrm{w}}$, $\varphi_y = 0$. At the planes of symmetry ($x = 0$ and $x = x_{\max}$): $u = v_x = T_x = \varphi_x = 0$. At the top of the computational domain (free surface, $y = y_{\max}$): $u_y = v_y = \varphi_y = 0$, $T = T_{\mathrm{sat}}$.

2.4. Numerical solution

The governing equations Eqs. (1)–(3), (7), and (8) combined together are highly nonlinear. The equations are discretized using finite difference method on a staggered grid system in which all the variables except pressure are stored at the grid points; and pressure alone is stored at the cell center as shown in Fig. 1. The diffusion terms are considered

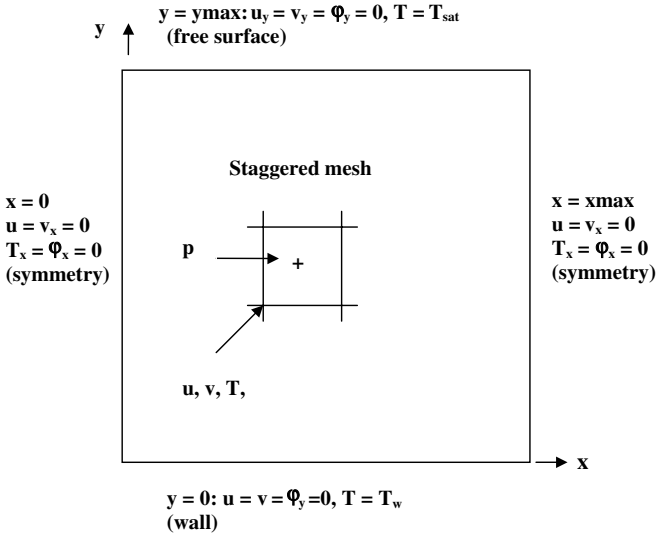

Fig. 2. Boundary conditions and the location of the variables stored in staggered grid system.

implicitly and the convection and source terms are considered explicitly in time. For spatial approximations all terms are considered using second-order central difference and the convection term by a second-order ENO method described by Chang et al. [22] to prevent numerical oscillations. The pressure and velocity are solved in a sequential manner by the procedure described in Selvam [23].

The discretized equations from the momentum, energy and pressure equations are symmetric and they are solved by the preconditioned conjugate gradient procedure (Ferziger and Peric [24]) in an iterative form. The iteration is done until the average residue for each node is reduced to less than 10^{-9}. This amount of accuracy is needed because of high density difference between liquid and vapor. After assuming initial position for distance functions, at each time-step the equations are solved sequentially in the following order:

(1) Solve the momentum equations, Eq. (1) for velocities.
(2) Correct the velocity to take the pressure effect.
(3) Solve the pressure Poisson equation to satisfy continuity.
(4) Update the velocities to include the new pressure effect.
(5) Solve temperature equation Eq. (2).
(6) Solve the distance function Eq. (7).
(7) Reinitialize the distance function as per Eq. (8) and go to next time step.

During the computation, time steps were chosen to satisfy the Courant–Fredreichs–Lewy (CFL) condition, $\Delta t \leqslant \min(h/(|u| + |v|), 10^{-6})$. This was done because of the explicit treatment of the convection terms and the condition that the numerical results should not change if the time steps are halved.

3. Results and discussion

Lin and Ponnappan [4] conducted spray cooling experiments using FC-72 for different T_{sat}. As an example $T_{sat} = 53$ °C case is considered. For this temperature, the computed reference values are: reference length $l_r = 736.2$ μm, reference velocity $u_r = 85$ mm/s, reference time $t_r = 8.66$ ms and $\Delta T = 10$ °C. The density ratio of liquid to vapor (ρ_l/ρ_v) is 138 and other nondimensional numbers are: $Re = 218$, $We = 1.0$, $Pe = 2050$ and $Ja = 0.127$. For initial study, the parameters considered are: $\rho_l/\rho_v = 20$, $Re = 200$, $We = 1.0$, $Pe = 1000$ and $Ja = 0.1$. Low density ratio is considered to reduce computer time and to avoid numerical instability. The computed results for higher density ratio has similar trend as low density ratio but the time step needs to be much smaller. Further study in the future will consider higher density ratios in detail.

Time steps considered are 5×10^{-6} (43.3 ns) and 1×10^{-6} (8.66 ns) nondimensional time. The computational domain considered are 0.1×0.1 units which is equal to 73.62×73.62 μm. The computational domain is discretized by 51×51 and 101×101 mesh at this time. The 101×101 mesh is considered to compare the results from 51×51 mesh and to evaluate the convergence. Most of the runs are made using 51×51 mesh. The smallest grid size varied from 0.7362 to 1.4724 μm.

3.1. Nucleation growth and merging of the vapor bubble

In a thin liquid film a growing bubble will merge with vapor over the liquid layer when the size is larger than the thickness of the film. In this section the process of growth and merging of vapor bubble is modeled. During the process the heat flux at the interface of liquid, vapor and wall is computed. For this case in the computational domain of 0.1×0.1 dimensionless unit 0.05 units of vapor layer is considered above the 0.05 units of liquid layer as shown in Figs. 3 and 6a. The total thickness of 0.1 units is equivalent to 73.62 μm. Grid sizes 51×51 and 101×101 are considered here for convergence study. The process of vapor bubble mixing with vapor on the top of the liquid film is a complex phenomenon where surface tension, phase change due to evaporation and gravity are interacting.

To accelerate the merging of the vapor bubble with vapor on the top layer an initial bubble radius of 0.03 to 0.04 units is considered for nucleation boiling. The liquid layer is considered up to 0.05 units of depth and beyond is assumed to be vapor. The distance function is assumed to vary from zero to positive value into the liquid from the interface of vapor bubble and liquid as well as from the interface of vapor layer and thin liquid film. The temperature is assumed to be varying linearly from T_w to T_{sat} from the wall to 0.01 units above the wall. Computation is done for 0.2 dimensionless time or 1.732 ms. Time steps considered are 5×10^{-6} (43.3 ns) and 1×10^{-6} (8.66 ns) nondimensional time. Total time steps varied from 40,000 for 43.3 ns time step to 200,000 for 8.66 ns time step.

The computed average *Nu* and the maximum velocity in the computational region with time are plotted in Figs. 4

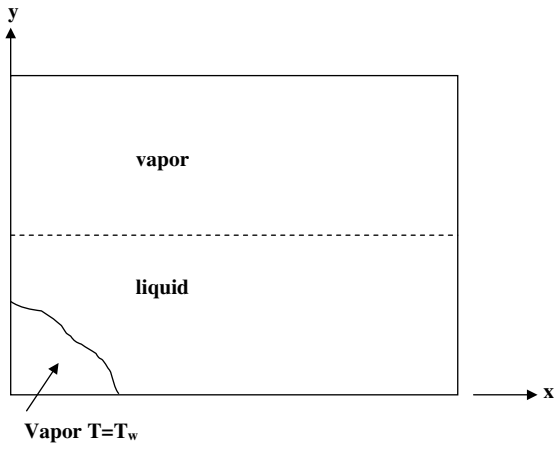

Fig. 3. Sketch showing the vapor bubble growing and vapor layer on the top of the liquid layer.

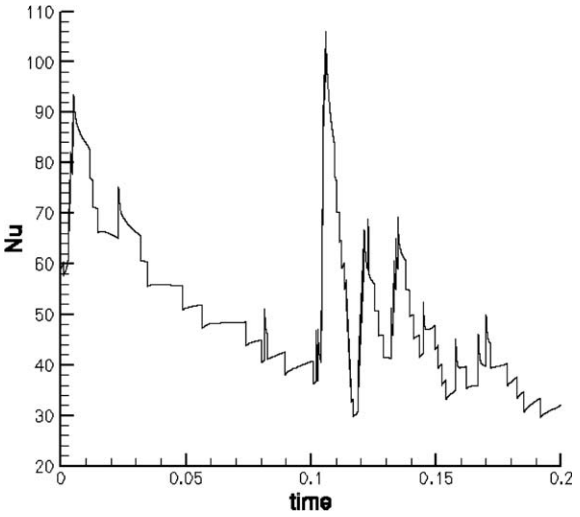

Fig. 4. Variation of Nusselt number with time for up to 1.732 ms.

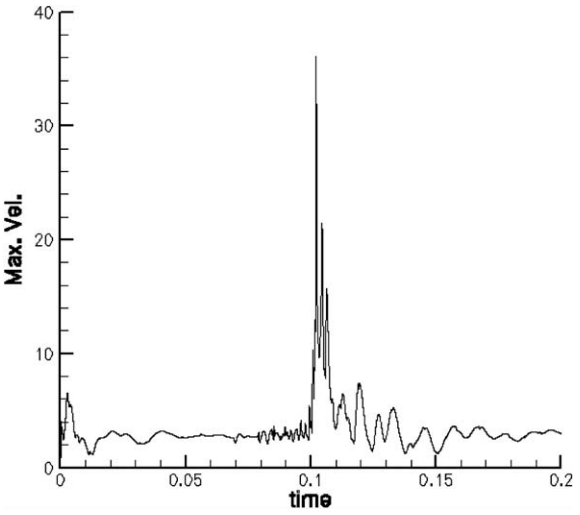

Fig. 5. Variation of maximum velocity in the computational region with time for up to 1.732 ms.

and 5. The average *Nu* decreases initially from 90 to 35 (until 0.1 dimesnionless time) during nucleate boiling of the bubble growth. After that the bubble merges with outside vapor. During this process the average Nu increases up to 106 sharply and then decreases to 30 in 0.02 dimensionless time (3.464 μs). After that also there are few jumps which are not as sharp as this one. At the same time in Fig. 5 one can see that the maximum velocity in the region increases from 3 to 36 units and comes back to 3 units. Hence when the vapor bubble merges with vapor on the top and the liquid finds its equilibrium position; the flow changes simultaneously in a very short time due to the interaction of the surface tension, viscosity, gravity and temperature. During this time the liquid spreads in the dry areas and hence there is an increase in average *Nu*. This is illustrated in time sequence using the velocity vector and temperature contour diagram for seven instant of time in Figs. 6 and 7. The time, average *Nu* and maximum velocity at which plots were made are reported in Table 1.

Using a 101×101 mesh the same computation is done in the same region of 0.1×0.1 units with a time step of 5×10^{-6} (43.3 ns). The computed maximum average *Nu* and velocity came to be 147.4 and 26.32 units compared to 106.1 and 36.11 units using 51×51 mesh. The grid spacing has impact on maximum *Nu* when cooler liquid spreads on the hot surface but it is difficult to consider the convergence study on *Nu*. The maximum velocity decreased due to grid refinement because there is more grid point available for the liquid and vapor interaction. Overall the flow features and variation of *Nu* with time have similar trend. When a time step of 1×10^{-6} (8.66 ns) is used on the 51×51 mesh the maximum *Nu* is 111.1. This is about 5% increase in the *Nu*. The computed maximum *Nu* and velocity using a 51×51 mesh with same time step for a liquid to vapor density ratio of 90 are 106 and 49.8. So this maximum *Nu* is the same as for density ratio of 20. On the other hand the velocity increased from 36.11 units to 49.8 units when the density ratio is increased. This is expected as the density ratio is increased the resistance due to vapor gets decreased.

The velocity vector and temperature contour diagrams for the corresponding time in Table 1 are reported in Fig. 6 and the variation of *Nu* along the wall for the same times is reported in Fig. 7. The maximum velocity in the computational region varies from 2 to 38 as plotted in Fig. 5 and it is very difficult to show such variations with same reference velocities in plots Fig. 6. In Fig. 6(a), (b) and (g) has same reference velocity for the plots and the rest of the figures the reference velocities are one tenth of the reference velocity used in Fig. 6(a), (b) and (g). It can be seen that the maximum average *Nu* is 92.91 at 927.53 μs and the maximum velocity is 11.16 at 891.16 μs which are less than the maximum reported in Figs. 4 and 5. The maximum velocity occurs when the bubble merges with the vapor layer around 0.102 (883.32 μs) dimensionless time and the maximum *Nu* occurs around 0.106 (917.96 μs) dimensionless time. Fig. 6(f) is close to the time of maximum *Nu* occurs. During this time it can be seen that the liquid is spread more than 0.07 units of the wall. Before the merger the liquid is spread less than 0.05 units. It is expected at 917.96 μs that the liquid could have spread more than 0.07 units and the thin layers could have evaporated. From Fig. 6(d)–(f) one can observe that the thermal boundary layer at the right boundary ($x = 0.1$ units) is almost similar. At the interface of liquid and vapor the thermal boundary layer is very thin in Fig. 6(f) and spread for 0.02 units more than Fig. 6(d). This is because the cooler liquid is slowly heated by conduction as explained by Selvam et al. [18]. In Fig. 7 one can see that maximum Nu is about 200 in Fig. 7(a)–(c) and once the bubble merges and liquid configuration changes it reaches as high as 450 in Fig. 7(e) and also peak value is spread much larger area than other plots. In other plots the *Nu* varies very sharply close to the maximum.

When the liquid is spreading with cooler liquid on the hot wall the *Nu* is high and distributed for some area. The sharp peaks are due to phase change on the side and the wider spread is due to phase change in the vertical direction. The maximum *Nu* reported in Fig. 7 are not the maximum occurring in the computation because we did not capture the time of maximum average *Nu*. This can be more than 500.

This study illustrates the importance of how the collapse of the vapor bubble in a rapid way helps to increase the heat transfer on the wall. The maximum average *Nu* reported in Fig. 4 is 106 whereas Lin and Ponnappan [4]

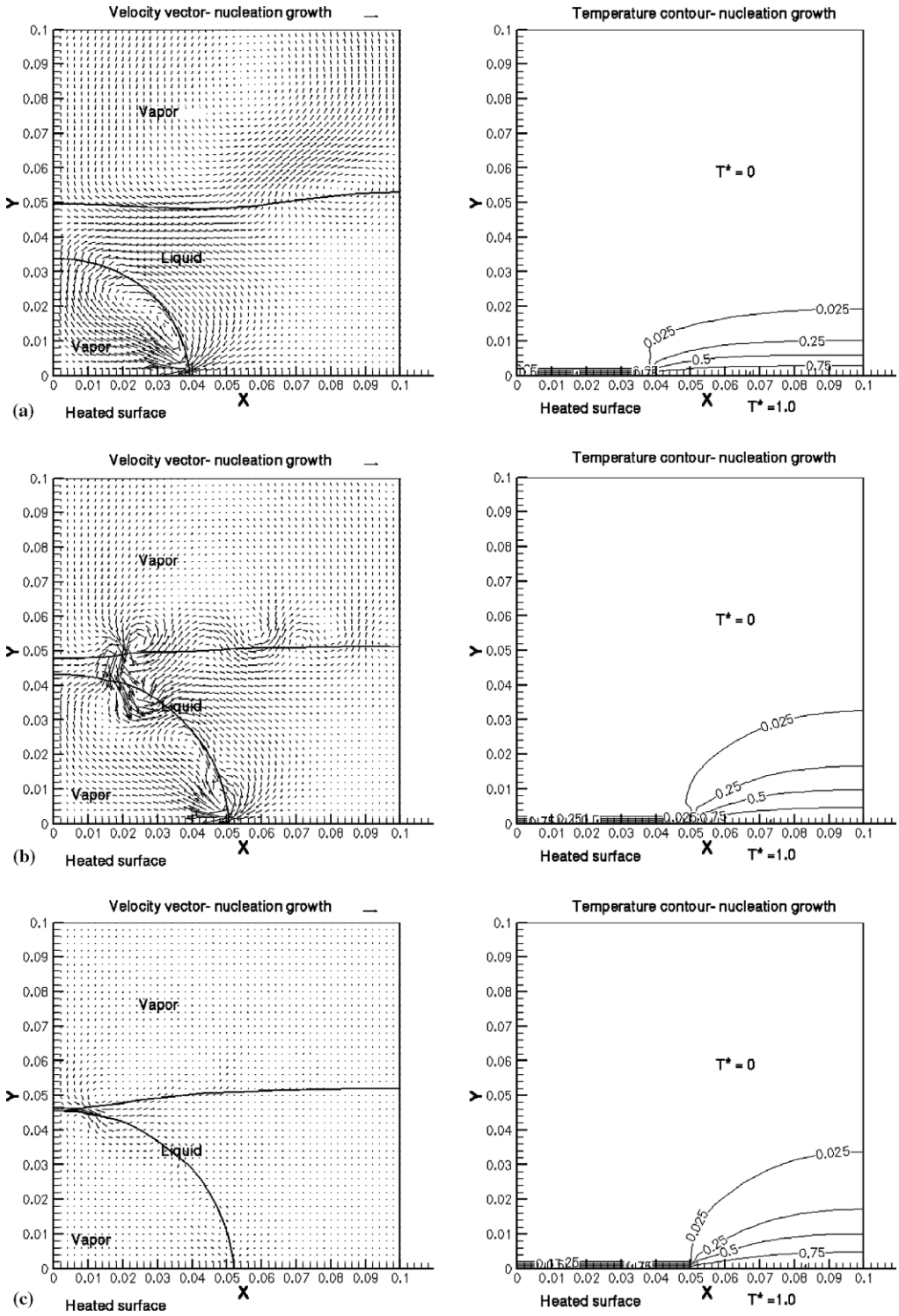

Fig. 6. Velocity vector and temperature contour diagrams during the merging of vapor bubble with vapor layer: (a) plot at 163.72 μs, (b) plot at 800.23 μs, (c) plot at 872.97 μs, (d) plot at 891.16 μs, (e) plot at 909.34 μs, (f) plot at 927.53 μs, (g) plot at 1727.71 μs.

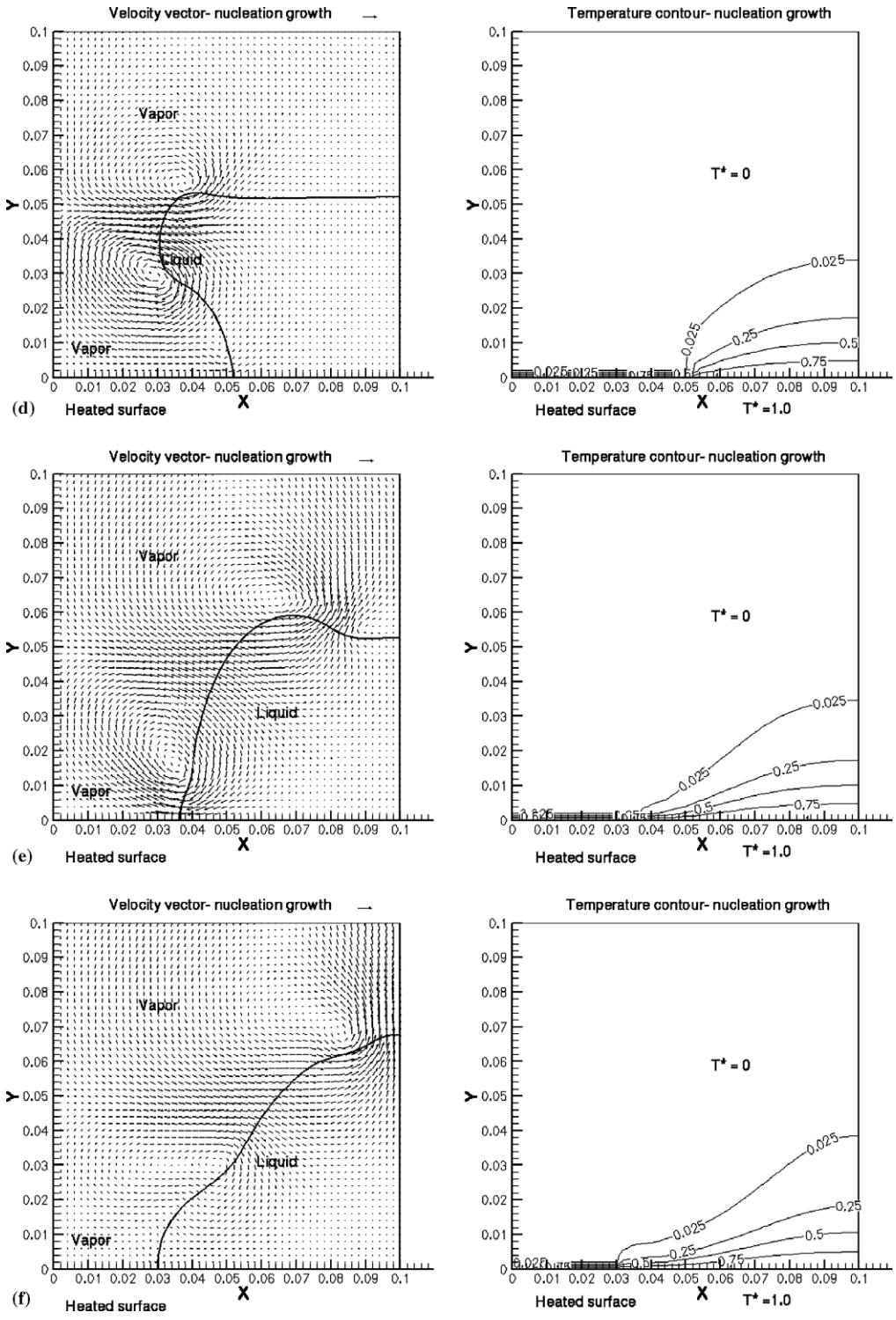

Fig. 6 (*continued*)

reported more than 200 in their experimental study. Here the collapse of the bubble due to merging with vapor layer is considered. In the actual spray cooling merging of vapor bubble with top layer, collapse of vapor bubbles due to impact of liquid droplet and convective flow of the liquid in the thin film all happens simultaneously in various proportions at different regions.

3.2. Modeling a droplet impact on thin liquid film

To study the impact of droplet on thin liquid film with vapor bubble growing, a vapor bubble with a radius of 0.055 (40.491 μm) units in a liquid layer of 0.06 (44.172 μm) units is considered as initial conditions as shown in Fig. 8. The initial temperature distribution is

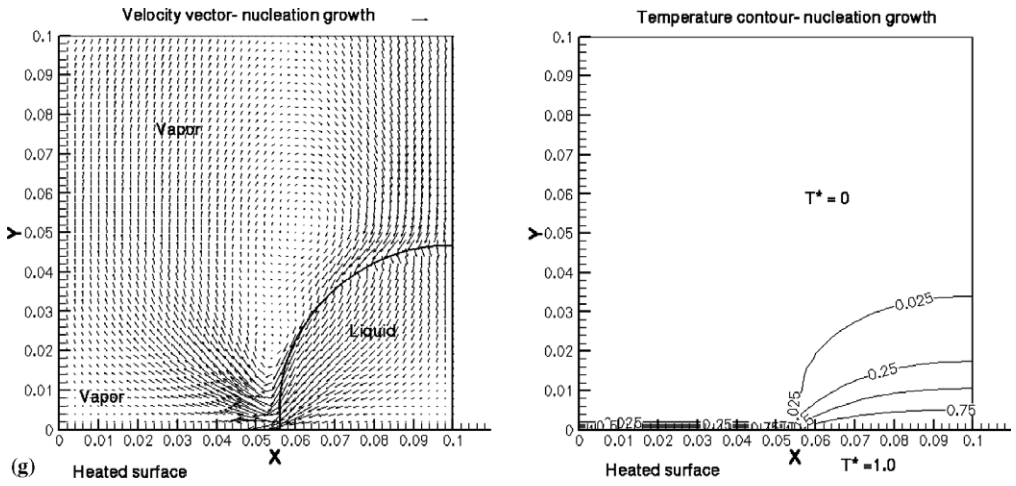

Fig. 6 (*continued*)

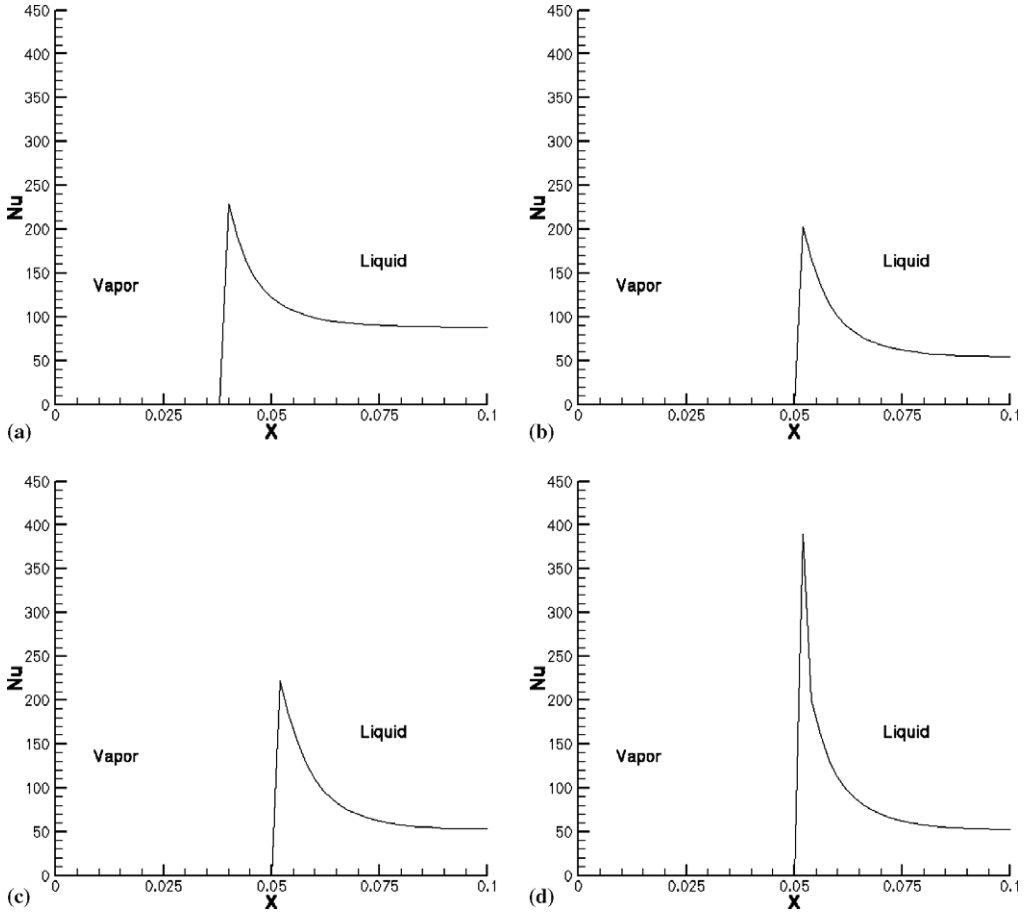

Fig. 7. Variation of Nusselt number along the hot surface at different times listed in Table 1: (a) plot at 163.72 μs and (b) plot at 800.23 μs, (c) plot at 872.97 μs and (d) plot at 891.16 μs, (e) plot at 909.34 μs and (f) plot at 927.53 μs, (g) plot at 1727.71 μs.

same as the merging of the vapor bubble case discussed in the previous discussion. A droplet diameter of 0.06 units falling down with a speed of 30 (2.55 m/s) units located at 0.13 (95.706 μm) units above the hot wall and 0.08 (58.896 μm) units from the left boundary is considered. These parameters are close to the 40 μm diameter of spray falling with a velocity of 10 m/s reported by Baysinger et al. [25] from experiment. The frequency of the falling droplet is suggested to be 1 kHz (1 ms interval) by Harris [26] from observation. The initial droplet temperature is assumed to be T_{sat}. The velocity of 2.55 m/s (30 units) considered in the numerical modeling is slightly lower than the 10 m/s. Even

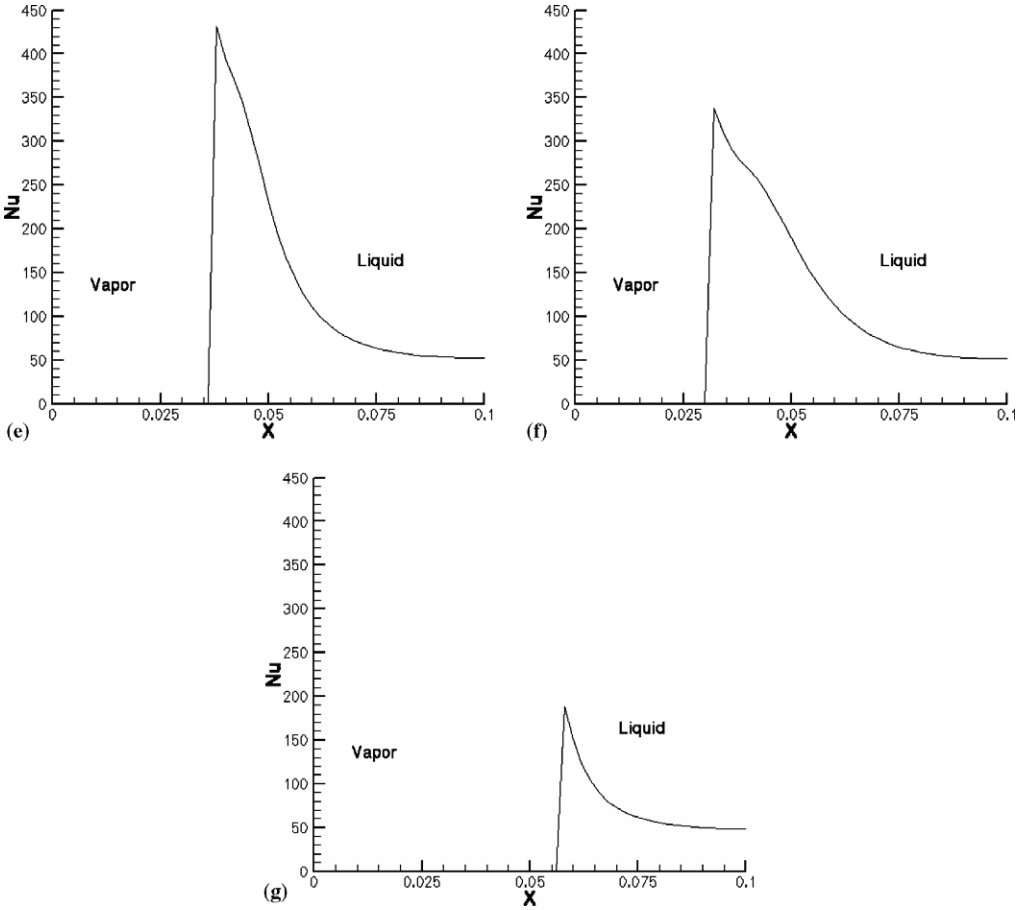

Fig. 7 (*continued*)

Table 1
Average *Nu* and maximum velocity for various times

Time (μs)	Average *Nu*	Maximum velocity (m/s)
0.018905 (163.72)	66.	2.93 (0.249)
0.092405 (800.23)	39.18	2.97 (0.252)
0.100805 (872.97)	40.81	10.21 (0.868)
0.102905 (891.16)	44.93	11.16 (0.949)
0.105005 (909.34)	88.14	10.72 (0.911)
0.107105 (927.53)	92.91	9.86 (0.838)
0.199505 (1727.71)	31.96	3.02 (0.257)

for the velocity of 30 units during impact, the maximum velocity in the computational region as shown in Fig. 9 increases up to 70 units which is the limit of the computational domain at this time. Further calculations with higher velocity will be done in the future. Due to impact, the velocity and flow change considerably and hence a computational domain of 0.2×0.2 units (147.24×147.24 μm) with 201×201 grid size is considered. Computation is done with a time step of 5×10^{-6} (43.3 ns) nondimensional time for 9000 time steps.

The computed flow patterns for the case of droplet falling right over the vapor bubble growing was reported in Selvam and Ponnappan [17]. Since the vapor bubble could not break due to droplet impact and merge with the vapor

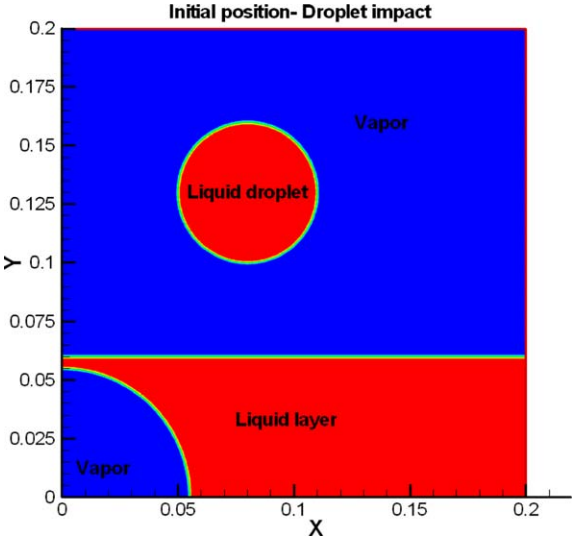

Fig. 8. Computational region for droplet impact.

on the top layer, the computed average Nu varied from 70 to 20. The heat transfer is similar to vapor bubble growth case reported in Selvam et al. [18]. When the droplet was falling over the thin liquid layer right above the bubble, the liquid droplet mixes with the thin layer and forms a thicker layer and hence the bubble could not break.

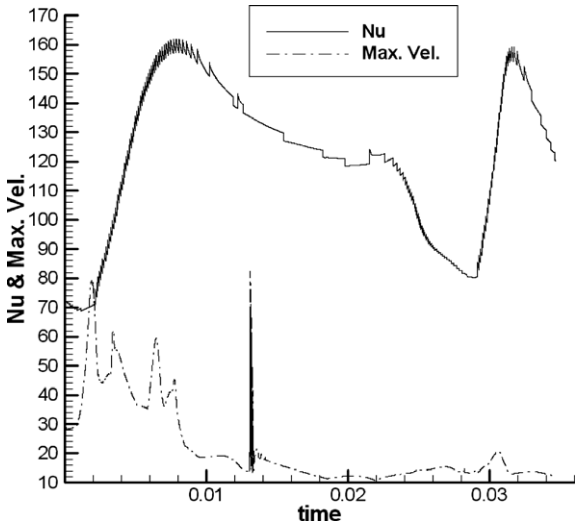

Fig. 9. Variation of average Nusselt number over the hot surface and maximum velocity in the computational region with time up to 0.036 units (311.76 μs).

The computed average *Nu* and the maximum velocity in the computational region with time are plotted in Fig. 9. The maximum velocity at each instant of time increases from 30 (2.55 m/s) units to close to 80 (6.8 m/s) units in 0.002 (17.32 μs) dimensionless time during the initial stages of the droplet impact. After that three more peaks appear but they are smaller than 80 (6.8 m/s) units. The *Nu* increase from 70 to 160 in 0.008 (69.28 μs) dimensionless time and then decreases to 80 at 0.03 (5.196 μs) dimensionless time. Then the *Nu* increases sharply to 160 in 0.002 (17.32 μs) dimensionless time and then decreases sharply as shown in Fig. 9. For high heat removal, the initial collapse of the vapor bubble due to impact is preferred because the *Nu* increases gradually and maintains high value much longer time than the later time when the liquid is trying to find the equilibrium with much slower motion. When the vapor bubble breaks due to impact the liquid and vapor trying to find equilibrium in a very short time and the flow and temperature changes in a very short time due to the interaction of the surface tension, viscosity, gravity, phase change due to temperature and transient conduction from the wall to liquid as in the merging of the vapor bubble case. Here due to impact of liquid droplet the heat removal capacity is much higher ($Nu = 160$ compared to $Nu = 100$) and the variation of *Nu* is spread much longer time (0.02 (173.2 μs) dimensionless time compared to 0.01 (86.6 μs) dimensionless time) than bubble merging case. For higher impact velocity much higher *Nu* may be expected. Further modeling work can help us to verify.

To illustrate systematically in time sequence, the effect of droplet impact on high heat removal, the shape of the liquid and vapor region during impact and the corresponding temperature contour are plotted for several instant of time in Fig. 10 and the variation of *Nu* along the wall for the same time is reported in Fig. 11. The time, average *Nu* and the maximum velocity at which plots were made are reported in Table 2. Fig. 10(a) is the plot after first time step. Because it is assumed that there is some initial temperature distribution in the liquid region the *Nu* is 70. After the liquid droplet impact on the liquid layer with vapor bubble the droplet spreads on the top of the liquid layer and at the same time the thin liquid layer above the bubble expands and tears away as shown in Fig. 10(b) after 31.61 μs. At the same time the temperature profile progress into liquid due to conduction and the liquid spreads into the dry area by 0.005 (3.681 μm) units at the bottom due to impact. Hence the average *Nu* reaches to 105.95 and the maximum *Nu* reaches to more than 900 as shown in Fig. 11(b). Due to impact, the cooler liquid starts spreading on the dry area where the vapor was growing as shown in Fig. 10(c) and the maximum *Nu* reaches to 920 as shown in Fig. 11(c). The corresponding average *Nu* reported in Table 2 is 160.46 at 63.48 μs. This high heat flux happens because of the transient conduction. The *Nu* is more than 200 in the region 0.015 (11.043 μm) to 0.05 (36.81 μm) units from the left boundary where the new liquid is spreading as shown in Fig. 11(c). In Fig. 10 (d) the liquid still spreads close to the left boundary but the average *Nu* ($133.54 < 160.46$) is less than the one in Fig. 10(c) because the new liquid is heated up and the heat flux or *Nu* got reduced as time goes on as shown in Fig. 11(d). The liquid that were expanding due to impact started to rebound as shown in Fig. 10(e) and the maximum *Nu* reduced to 100 as shown in Fig. 11(e). Then the liquid spreads one more time in the dry area towards the left boundary as shown in Fig. 10(f). This new liquid again shoots the average *Nu* to 159.11 and maximum *Nu* in Fig. 11(f) to 980. Thus it is clearly illustrated from this study that the liquid droplet impact moves cooler liquid to the dry heated area and because of that very high heat flux (q) are achieved due to transient heat conduction. For much higher velocity higher average *Nu* can be achieved. Further study is underway to investigate the effect of droplet size, velocity and thickness of liquid layer on heat transfer.

3.3. Mechanism of spray cooling

When the vapor bubble breaks due to liquid droplet impact the cooler liquid spreads in the dry hot area and heat is conducted from the wall to the liquid layer. This transient conduction in a very short time is the one produces the high heat flux as explained in Selvam et al. [18]. During transient conduction from a heated wall with constant surface temperature of T_w, the heat flux is inversely proportional to the square root of time and for constant surface heat flux the change in temperature is directly proportional to the square root of time as derived in any standard text [27]. So during very short time high heat flux is produced during conduction from the wall to liquid. But to bring cooler liquid to the heated surface in a very short time, vapor bubble collapse due to impact is necessary. In spray cooling this happens due to phase change of the liquid to vapor and droplet impact.

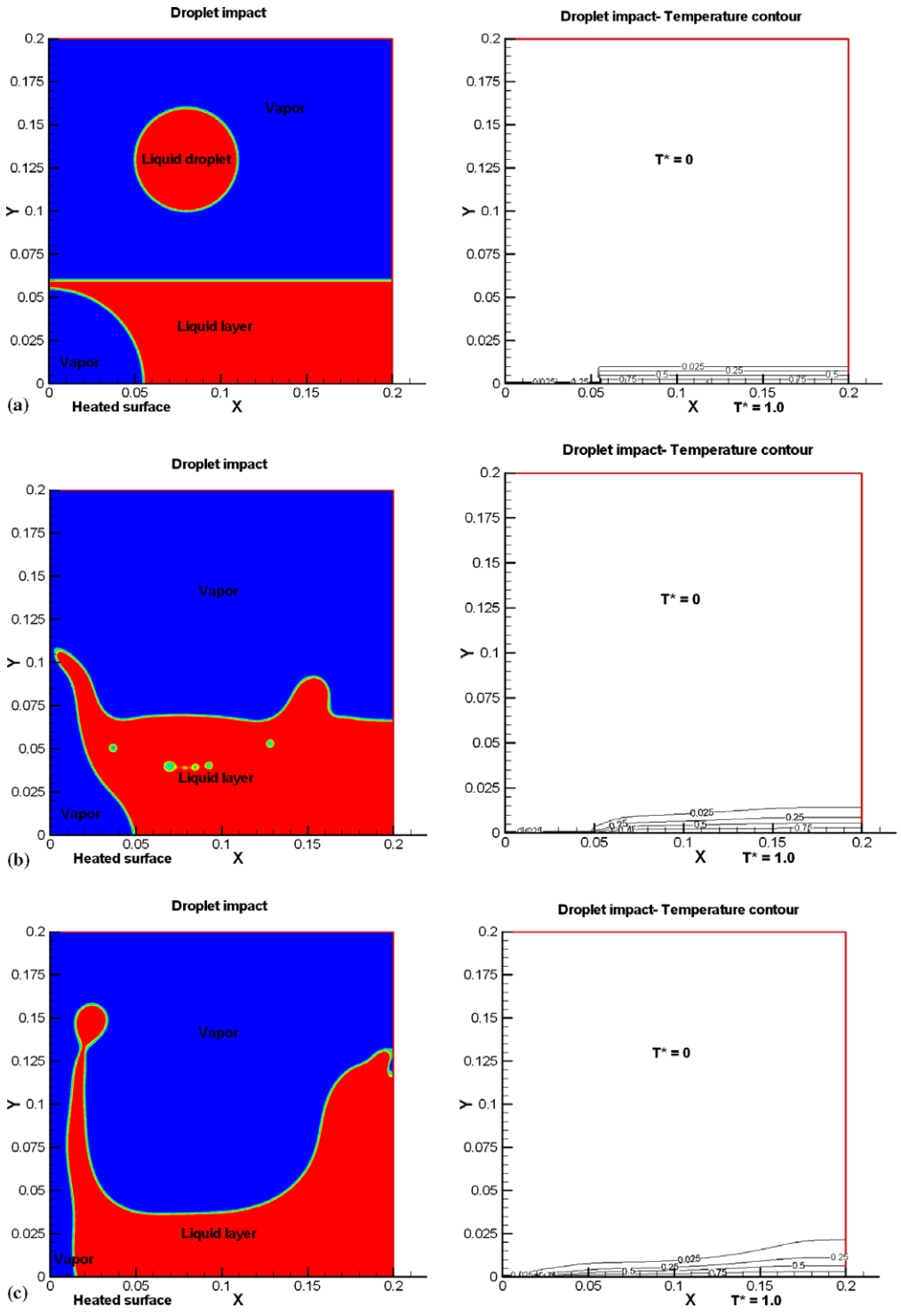

Fig. 10. Shape of the liquid and vapor layer at different times during droplet impact: (a) plot at 0.043 μs, (b) plot at 31.61 μs, (c) plot at 63.48 μs, (d) plot at 118.64 μs, (e) plot at 244.21 μs, (f) plot at 274.52 μs.

4. Conclusions

Numerical modeling of multiphase flow in spray cooling using level set method is discussed. The model considers the effect of surface tension between liquid and vapor, gravity, phase change and viscosity. The computer model is used to study the spray cooling phenomenon in the micro environment of about 40 μm thickness liquid layers with vapor bubble growing due to nucleation. The importance of studying the heat transfer mechanism in thin liquid film for spray cooling is identified. The flow and heat transfer details are presented for two cases: (1) when the vapor bubble grows due to nucleation and (2) merges with the vapor layer above the liquid layer and when a liquid

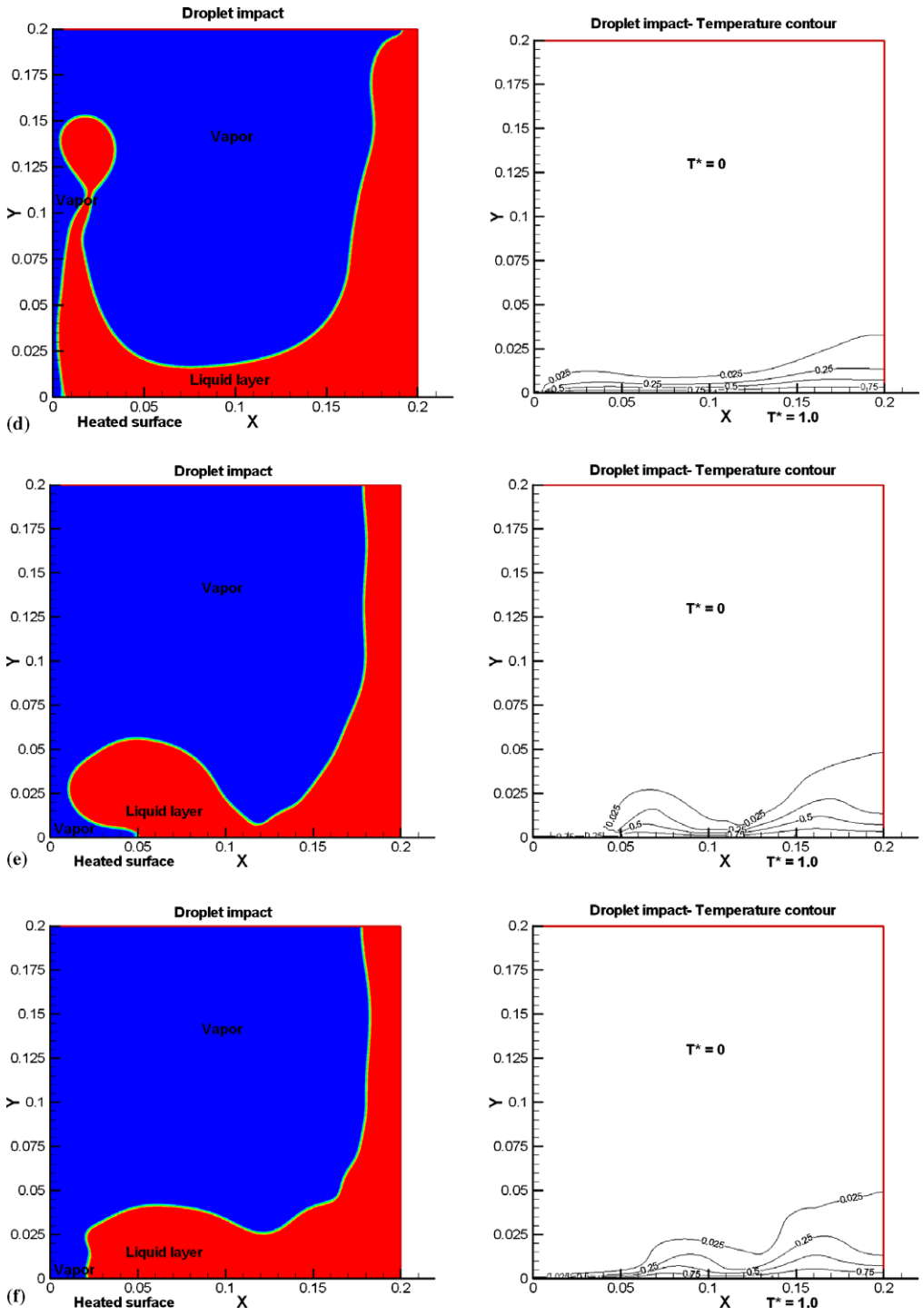

Fig. 10 (*continued*)

droplet impacts the thin liquid layer with vapor bubble growing. From the study the following conclusions are made:

1. For high heat flux spray cooling, the thin film on the heated surface and its interaction with liquid droplet are very important.
2. The collapse of the vapor bubble in liquid layer either by liquid droplet impacting at high speed and the vapor bubble breaking during merging of vapor on the top of the thin liquid film have major impact on spray cooling heat transfer.
3. The complex interaction of conduction of the heat from the heated surface into liquid and convection of the liquid during sudden impact due to droplet or breaking of vapor bubble and formulation of vapor bubble due to phase change are identified to be the major phenomena in spray cooling.

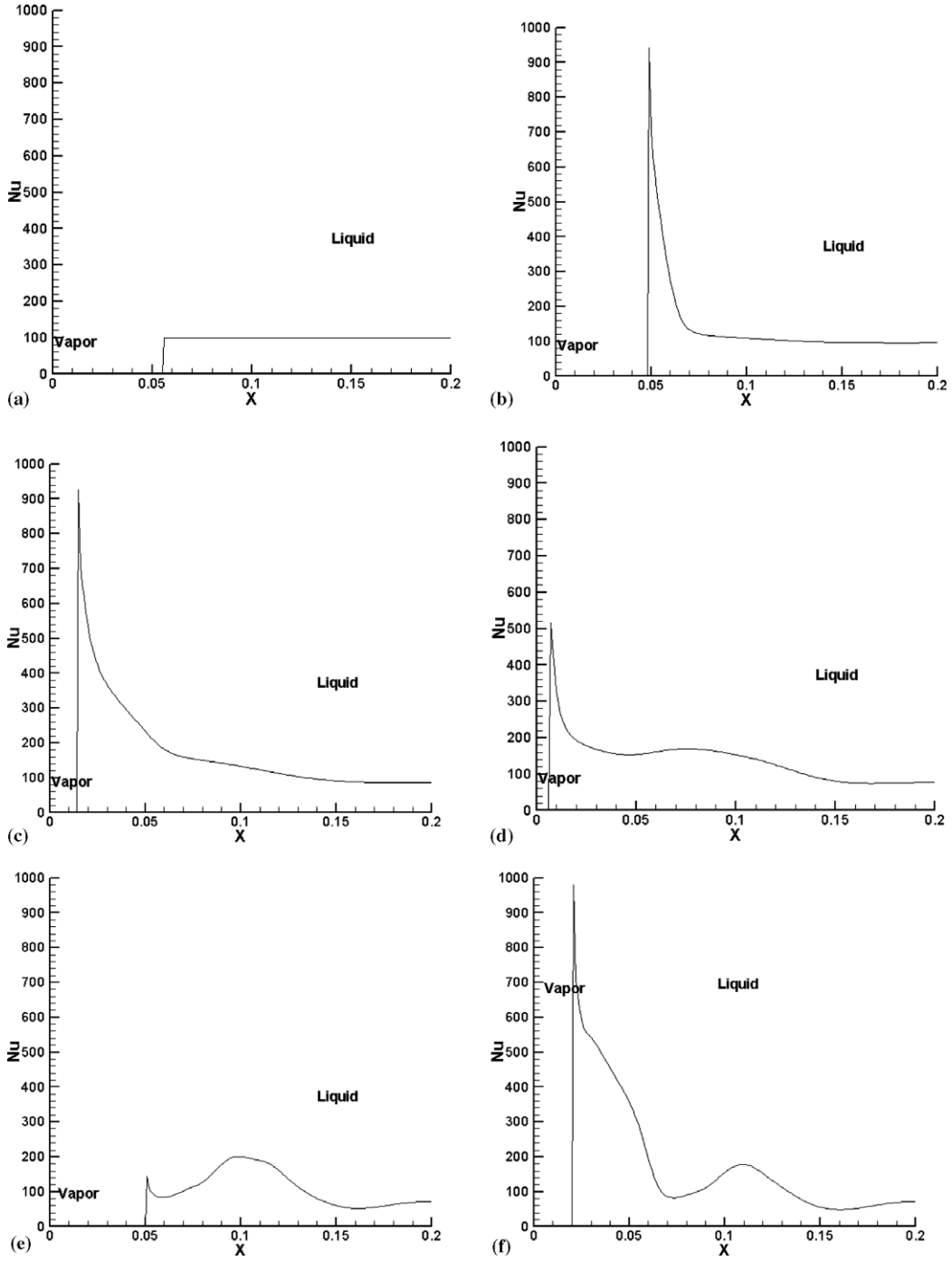

Fig. 11. Variation of Nusselt number along the hot surface at different times listed in Table 2: (a) plot at 0.043 μs and (b) plot at 31.61 μs, (c) plot at 63.48 μs and (d) plot at 118.64 μs, (e) plot at 244.21 μs and (f) plot at 274.52 μs.

Table 2
Average *Nu* and maximum velocity for various times during droplet impact

Time (μs)	Average *Nu*	Maximum velocity (m/s)
5×10^{-6} (0.043)	72.88	44.35 (3.77)
0.00365 (31.61)	105.95	55.34 (4.70)
0.00733 (63.48)	160.46	40.32 (3.43)
0.0137 (118.64)	133.54	18.38 (1.56)
0.0282 (244.21)	81.57	14.60 (1.24)
0.0317 (274.52)	159.11	13.05 (1.11)

Table 3
Comparison of maximum average *Nu* and maximum velocity for different case study

Description	Average *Nu*	Velocity
Vapor bubble growth (Selvam and Ponnappan [17])	50	3 units (0.255 m/s)
Bursting of bubble (Section 3.1)	110	36 units (3.06 m/s)
Droplet impact	160	80 units (6.8 m/s)

4. The importance of moving the cooler liquid quickly to heated dry surface which causes the high heat flux due to transient conduction is recognized. This is explained with temperature contour and heat flux (q) plots at different times.
5. The comparison of maximum average *Nu* and the maximum velocity in the computational region for different cases is reported in Table 3. From the table one can conclude that maximum velocity in the liquid created due to impact moves the liquid on dry hot surface and hence high heat flux are created. When there is only phase change due to bubble growth the maximum average *Nu* is 50, whereas due to droplet impact on the vapor bubble the maximum average *Nu* reached 160.
6. Further study is recommended to study the effect of size and velocity of the droplet and thickness of the liquid layer on heat removal capacity.

Acknowledgements

This work was conducted at the AFRL/WPAFB Propulsion Directorate's Power Division, Thermal Laboratory during the summer of 2004. The first author acknowledges the support received from the US Air Force Research Lab through the Universal Technology Corporation's summer faculty program contract F33615-02-D-2299 and the ONR/DEPSCoR grant through the University of Arkansas to perform this work and the encouragement provided by Dr. Juan Balda, Dr. Fred Barlow and Dr. Aicha Elshabini, Department of Electrical Engineering, University of Arkansas to visit WPAFB during the summer of 2004.

References

[1] J. Yang, L.C. Chow, M.R. Paris, Nucleate boiling heat transfer in spray cooling, J. Heat Transfer 118 (1996) 668–671.
[2] L.C. Chow, M.S. Sehembey, M.R. Paris, High heat flux spray cooling, Ann. Rev. Heat Transfer 8 (1997) 291–318.
[3] I. Mudawar, Assessment of high heat-flux thermal management schemes, IEEE Trans. Comp. Packag. Technol. 24 (2001) 122–141.
[4] L. Lin, R. Ponnappan, Heat transfer characteristics of spray cooling in a close loop, Int. J. Heat Mass Transfer 46 (2003) 3737–3746.
[5] M. Sussman, P. Smereka, S. Osher, A level set approach for computing solutions to incompressible two-phase flow, J. Comp. Physics 114 (1994) 146–159.
[6] G. Trggvason et al., A front-tracking method for the computations of multiphase flow, J. Comp. Physics 169 (2001) 708–759.
[7] G. Son, V.K. Dhir, Numerical simulation of film boiling near critical pressures with a level set method, J. Heat Transfer 120 (1998) 183–192.
[8] G. Son, N. Ramanujapu, V.K. Dhir, Numerical simulation of bubble merger process on a single nucleation site during pool nucleate boiling, J. Heat Transfer 124 (2002) 51–62.
[9] H.Y. Yoon, S. Koshizuka, Y. Oka, Direct calculation of bubble growth, departure, and rise in nucleate pool boiling, Int. J. Multiphase Flow 27 (2001) 277–298.
[10] S.W.J. Welch, J. Wilson, A volume of fluid based method for fluid flows with phase change, J. Comp. Physics 160 (2000) 662–682.
[11] X.Y. Luo, M.J. Ni, A. Ying, M.A. Abadou, Numerical modeling for multiphase incompressible flow with phase change, Numer. Heat Transfer, Part B 48 (2005) 425–444.
[12] M. Pasandideh-Fard, S.D. Aziz, S. Chandra, J. Mostaghimi, Cooling effectiveness of water drop impinging on hot surface, Int. J. Heat Mass Transfer 22 (2001) 201–210.
[13] J.P. Kizito, et al., Numerical and experimental studies of splashing droplets, AIAA-2004-0960, 42nd AIAA Aerospace Science Meeting and Exhibit, 2004.
[14] M. DiMarzo et al., Evaporative cooling due to a gravity deposited droplet, Int. J. Heat Mass Transfer 36 (1993) 4133–4139.
[15] Y. He, M. Shoji, S. Maruyama, Numerical study of high heat flux pool boiling heat transfer, Int. J. Heat Mass Transfer 44 (2001) 2357–2373.
[16] J. Kern, P. Stephan, Theoretical model for nucleate boiling heat and mass transfer of binary mixtures, J. Heat Transfer 125 (2003) 1106–1115.
[17] R.P. Selvam, R. Ponnappan, Numerical modeling of nucleation boiling in thin film and effect of droplet impact, in: Proceedings of the 15th Annual Thermal & Fluids Analysis Workshop (TFAWS 2004), Pasadena, CA, August 30th to September 3rd, 2004.
[18] R.P. Selvam, L.Lin, R. Ponnappan, Computational modeling of spray cooling: current status and future challenges, in: Proceedings of the Space Technology and Applications International Forum (STAIF 2005), Conference on Thermophysics in Microgravity, Albuquerque, NM, February 13–17, 2005
[19] J.A. Sethian, Level Set Methods and Fast Marching Methods: Evolving Interfaces in Computational Geometry, Fluid Mechanics, Computer Vision and Materials Science, Cambridge University Press, Cambridge, UK, 1999.
[20] S. Osher, R. Fedkiw, Level Set Methods and Dynamic Implicit SurfacesApplies Mathematical Sciences, Vol. 153, Springer, New York, 2003.
[21] J.U. Brackbill, D.B. Kothe, C. Zamach, A continuum method for modeling surface tension, J. Comp. Phys. 100 (1992) 335–354.
[22] Y.C. Chang, T.Y. Hou, B. Merriman, S. Osher, A level set formulation of Eulerian interface capturing methods for incompressible fluid flows, J. Comp. Phys. 124 (1996) 449–464.
[23] R.P. Selvam, Computation of pressures on Texas Tech building using large eddy simulation, J. Wind Eng. Ind. Aerodyn. 67 & 68 (1997) 647–657.
[24] J.H. Ferziger, M. Peric, Computational Methods for Fluid Dynamics, Springer, New York, 2002.
[25] K.M. Baysinger et al., Design of a microgravity spray cooling experiment, AIAA-2004-0966, 42nd AIAA Aerospace Sciences Conference and Exhibit, January 5–8, Reno, NV, 2004.
[26] R.J. Harris, Private Communications, University of Dayton Research Institute, Dayton, OH, 2004.
[27] F.P. Incropera, D.P. DeWitt, Fundamentals of Heat and Mass Transfer, fourth ed., John Wiley & Sons, New York, 1996.